Int J Thermophys (2016) 37:74
DOI 10.1007/s10765-016-2079-4

ICPPP 18

SNR and Contrast Enhancement Techniques for the Photoacoustic Radar Imaging

Wei Wang[1] · **Andreas Mandelis**[1]

Received: 10 October 2015 / Accepted: 14 May 2016 / Published online: 1 June 2016

Abstract This paper presents two methods for photoacoustic signal enhancement in biological tissues. One such method is based on the fact that temperature can affect the signals of the photoacoustic radar. Therefore, thermally assisted methods have been used for photoacoustic imaging contrast improvement. Another method is based on harmonic wavelength modulation which results in a differential PA radar signal to strengthen early cancer detection. Two chirped waveforms modulated out-of-phase between 680 nm and 800 nm can effectively suppress the background noise, greatly enhance the SNR and detect small variations in hemoglobin oxygenation levels, thereby distinguishing pre-malignant tumors. Experimental results demonstrate the accuracy of the frequency-modulated differential measurement with sheep blood at different hemoglobin oxygenation (S_tO_2) levels.

Keywords Hemoglobin oxygenation · Imaging contrast · Photoacoustic imaging · Signal-to-noise ratio

1 Introduction

Early cancer detection can reduce death rate when followed by treatment and the detected tumors can only be effectively treated before metastases (spreading to other organs or parts) [1]. In recent years, photoacoustic (PA) imaging has been introduced

This article is part of the selected papers presented at the 18th International Conference on Photoacoustic and Photothermal Phenomena.

✉ Wei Wang
weiwang@mie.utoronto.ca

[1] Department of Mechanical and Industrial Engineering, Center for Advanced Diffusion Wave Technologies (CADIFT), University of Toronto, Toronto M5S3G8, Canada

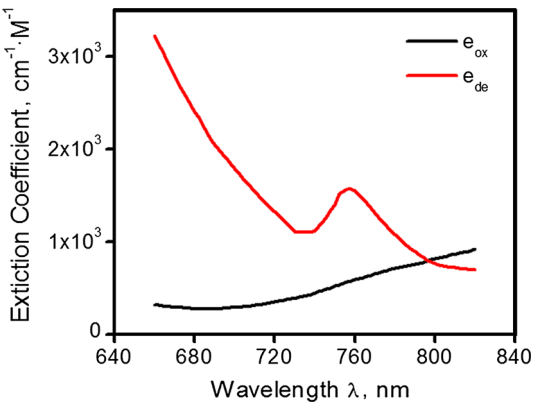

Fig. 1 Absorption spectra of hemoglobin expressed as extinction coefficient of oxy-hemoglobin e_{ox} and deoxy-hemoglobin e_{de}

for early cancer detection. The PA technique is based on the detection of acoustic signals generated by light absorption in tissue which combines the advantages of high contrast due to light absorption with high resolution and penetration depth of the ultrasound signal. The PA imaging system has good sensitivity, resolution, and contrast, but the major limitation is the penetration of light [2]. Light intensity decreases exponentially with penetration depth because of strong scattering and absorption in biological tissues [3,4]. Signal-to-noise ratio (SNR) and imaging contrast are important issues of PA imaging systems.

The widely accepted normal body temperature for a healthy adult is 37 °C approximately [5]. Studies show that most normal tissues such as muscles, kidney, and liver can withstand temperatures up to 44 °C for 30 min [6–8]. Temperature can affect PA signals: the PA signal is stronger at higher temperatures [9,10].

The maximum difference between molar extinction coefficients of oxy- and deoxy-Hb occurs at 680 nm, while they coincide near 800 nm as shown in Fig. 1 [11]. Therefore, the PA signal is more sensitive to changes of blood parameters at 680 nm than 800 nm. The frequency-domain photoacoustic system noise background can be significantly suppressed when the two modulating signals are out of phase, and the difference between those two signals is amplified. Therefore, the differential PA signals at two wavelengths can measure very small changes with better sensitivity. Inadequate hemoglobin oxygen levels (tissue hypoxia) can compromise tissue functions [12]. Measurement of tissue oxygen saturation (S_tO_2) is useful for peripheral arterial disease assessment [13] and has been reported for peripheral arterial disease assessment [13]. Monitoring hemoglobin oxygenation level in real time is an important method for cancer diagnosis [12]. Pulsed-PA-signal has been used for blood oxygenation [14].

In this study, we present two techniques for contrast and SNR enhancement of a PA radar imaging system: a thermally assisted method for PA imaging contrast, and a differential measurement method for SNR measurement sensitivity improvement.

2 Theoretical Background

The photoacoustic radar uses modulated continuous wave (CW) laser beams which, upon absorption, generate temperature oscillations in a sample and produce ther-

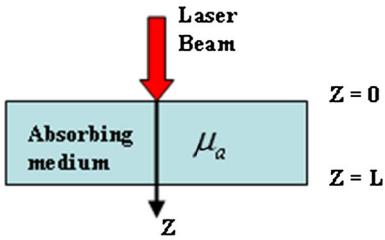

Fig. 2 PA source geometry with light absorption

moelastic acoustic pressure oscillations. The response spectrum $\tilde{\varphi}(\vec{r}, \omega)$ of the acoustic velocity potential in an absorbing medium is generated by the spatially distributed energy source fluence $\tilde{E}(\vec{r}, \omega)$ $(\mathrm{J} \cdot \mathrm{Hz} \cdot \mathrm{m}^{-2})$ and can be described by the Helmholtz equation [15]:

$$\nabla^2 \tilde{\varphi}(\vec{r}, \omega) + k_a^2 \tilde{\varphi}(\vec{r}, \omega) = \frac{\beta \mu_a}{\rho c_p} \tilde{E}(\vec{r}, \omega) \tag{1}$$

where $k_a = \omega / c_a$ $(\mathrm{rad} \cdot \mathrm{m}^{-1})$ is the acoustic angular wavenumber, ω $(\mathrm{rad} \cdot \mathrm{s}^{-1})$ represents the angular modulation frequency, μ_a (m^{-1}) is the light absorption coefficient, β $(^{\circ}\mathrm{C}^{-1})$ is the volume thermal expansion coefficient, ρ $(\mathrm{kg} \cdot \mathrm{m}^{-3})$ is the density, c_a $(\mathrm{m} \cdot \mathrm{s}^{-}1)$ is the speed of sound, and c_p $(\mathrm{J} \cdot \mathrm{kg}^{-}1 \cdot {}^{\circ}\mathrm{C})$ is the specific heat capacity at constant pressure. In the one-dimensional case, laser light is incident normally to the surface of an absorbing medium as shown in Fig. 2. The light fluence reaching subsurface depth in the medium can be estimated by

$$\tilde{E}(z, \omega) = e^{-\mu_{ef} z} \tilde{E}_0(\omega), \tag{2}$$

where $\tilde{E}_0(\omega)$ is the light fluence at the surface of absorber, $\tilde{E}(z, \omega)$ is the Fourier transform of fluence at the specific location z of the absorber, and μ_{ef} is the effective light attenuation coefficient. The effective light attenuation coefficient in the presence of scattering is defined as [3]

$$\mu_{ef} = \sqrt{3\mu_a(\mu_a + \mu_s')}, \tag{3}$$

where μ_s' is the reduced light scattering coefficient, and is defined by

$$\mu_s' = \mu_s(1 - g), \tag{4}$$

where μ_s is the light scattering coefficient (m^{-1}), and g is the scattering anisotropy. The anisotropy is a factor measuring the cosine of the scattering angle, and defines the scattering directional probability. Equation 1 is written in one dimension as

$$\frac{d^2}{dz^2} \tilde{\varphi} + k_a^2 \tilde{\varphi} = \frac{\beta \mu_a}{\rho c_p} \tilde{E}(z, \omega). \tag{5}$$

The general solution of the second order differential equation of Eq. 5 is given by [15]

$$\tilde{\varphi}(z,\omega) = C_+ e^{j(\omega/c_a)z} + C_- e^{-j(\omega/c_a)z} + \frac{\beta}{\rho c_p}\frac{\mu_a}{\mu_a^2 + \omega^2/c_a^2}\tilde{E}(z,\omega). \tag{6}$$

The first two terms describe the acoustic waves traveling forward or backward inside the medium. The last term in Eq. 6 is the driving term. It diminishes exponentially with increasing depth and is considered as zero for $\mu_a z \geq 5$. In the case where no wave travels toward the boundary medium with a rigid boundary condition, so $C_- = 0$, and with the rigid boundary approximation, on the surface of the medium $z = 0$, the velocity is given as

$$v_{z=0} = \left.\frac{\partial\tilde{\varphi}}{\partial z}\right|_{z=0} = 0 \tag{7}$$

Substituting Eqs. 7 into 6, C_+ gives

$$C_+ = -j\frac{c_a}{\omega}\frac{\beta}{\rho c_p}\frac{\mu_a\mu_{ef}}{\mu_a^2 + \omega^2/c_a^2}\tilde{E}_0(\omega). \tag{8}$$

Using pressure $\tilde{p} = j\rho\omega\tilde{\varphi}$, and substituting C_+ into Eq. 6, the pressure spectrum $\tilde{p}(z,\omega)$ can be written as

$$\tilde{p}(z,\omega) = \frac{\beta c_a^2}{c_p}\frac{\mu_a}{\mu_a c_a + j\omega}e^{-(\mu_{ef}+j\omega/c_a)z}\tilde{E}_0(\omega). \tag{9}$$

Therefore, the amplitude spectrum of $\tilde{p}(\vec{z},\omega)$ can be obtained as

$$|\tilde{p}(z,\omega)| = \frac{\mu_a\beta c_a^2 e^{-\mu_{ef}z}}{c_p\sqrt{\mu_a^2c_a^2+\omega^2}}\tilde{E}_0(\omega) = \frac{\mu_a\Gamma e^{-\mu_{ef}z}}{\sqrt{\mu_a^2c_a^2+\omega^2}}\tilde{E}_0(\omega), \tag{10}$$

where $\Gamma = \frac{\beta c_a^2}{c_p}$ is the Gruneisen parameter. Gruneisen parameter is a temperature-dependent parameter, thus PA signal changes with temperature [9].

For laser A at 680 nm wavelength, the light absorption coefficient is labeled μ_a^A, and the generated signal is $\tilde{p}_A$. For laser B at 800 nm wavelength with light absorption coefficient labeled μ_a^B, the phase is shifted 180° with respect to laser A, and the generated signal is $\tilde{p}_B$. Other parameters are the same as laser A. When the generated PA signals by laser A and laser B are superimposed, the differential signal $\tilde{p}_{AB}(z,\omega)$ is expressed as

$$\tilde{p}_{AB}(z,\omega) = \tilde{p}_A(z,\omega) + \tilde{p}_B(z,\omega) \tag{11}$$

We can write the differential signal $\tilde{p}_{AB}(z,\omega)$ as follows:

$$\tilde{p}_{AB}(z,\omega) = \left[\frac{\Gamma\mu_a^A \tilde{E}_A(z,\omega)}{\sqrt{\left(\mu_a^A\right)^2 c_a^2 + \omega^2}} - \frac{\Gamma\mu_a^B \tilde{E}_B(z,\omega)}{\sqrt{\left(\mu_a^B\right)^2 c_a^2 + \omega^2}}\right](\cos\phi_A + j\sin\phi_A), \quad (12)$$

where ϕ_A is given as

$$\phi_A = \tan^{-1}\left(\frac{\omega\cos(\frac{\omega z}{c_a}) + \mu_a^A c_a \sin(\frac{\omega z}{c_a})}{\omega\sin(\frac{\omega z}{c_a}) - \mu_a^A c_a \cos(\frac{\omega z}{c_a})}\right). \quad (13)$$

The PA radar uses a matched-filter pulse compression method for signal processing, in order to give the PA signal depth information and adequate SNR. The matched-filter output is

$$R(t) = \int_{-\infty}^{+\infty} s(\tau)\cdot r(t+\tau)d\tau = \Im^{-1}\left\{\tilde{s}(\omega)\cdot\tilde{r}^*(\omega)\right\}, \quad (14)$$

where $s(t)$ and $r(t)$ are the detected signal and the reference signal, respectively, and $\Im^{-1}$ denotes the inverse Fourier transformation.

3 Experimental Results and Discussion

Figure 3 shows the experimental setup for PA imaging with a 64-element phased array transducer (Ultrasonix Medical Corp, frequency range from 2 MHz to 4 MHz

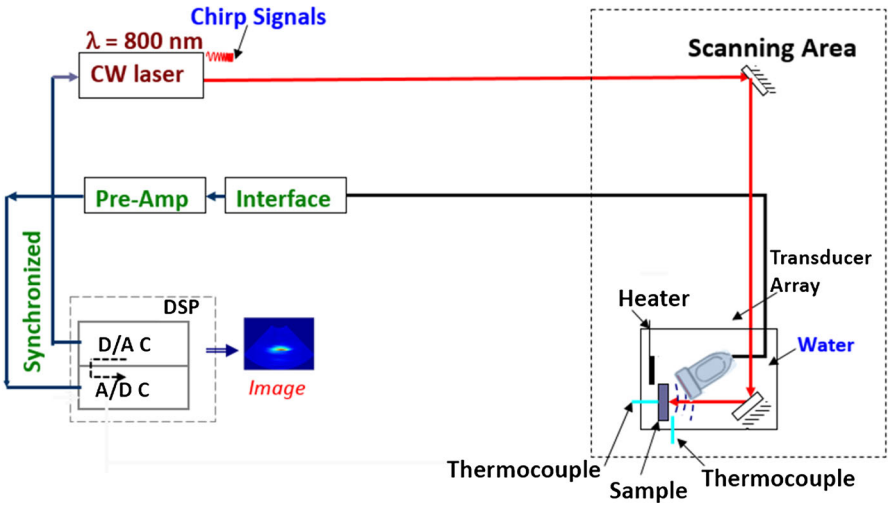

Fig. 3 Experimental setup for PA radar imaging with a transducer array

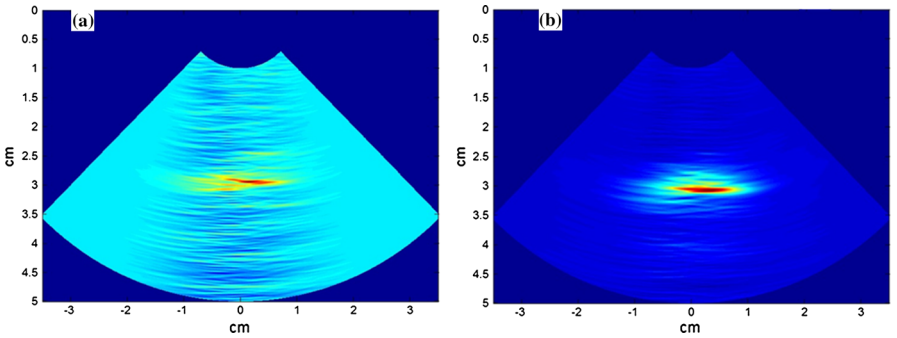

Fig. 4 (a) Image generated at 32 °C, $CF = 2.7$; (b) Image generated at 38 °C, $CF = 3.2$

and 0.254 mm pitch). The laser beam was modulated using LFM chirps (0.5 to 4 MHz, 1ms long) generated by a signal generation card (NI PXI-5442). Figure 4a and b show the images generated by PA signals at different temperatures. At 38 °C, a higher contrast image was generated than the image at 32 °C. The sample was a PVCP phantom. The image contrast can be measured by means of a contrast factor (CF) as [16]

$$CF = \frac{Signal_{absorber} - Signal_{background}}{Signal_{background}}. \tag{15}$$

The averaged signals were used for CF calculation. The evaluated CF is 2.7 at 32 °C for the image in Fig. 4a, and 3.2 at 38 °C for the image in Fig. 4b.

The experimental setup for differential photoacoustic radar spectroscopy is shown in Fig. 5a. The two aforementioned lasers A and B were modulated by two out-of-phase linear frequency chirp signals (sweep from 0.3 MHz to 2.6 MHz in one millisecond). The chirp signals were generated by a dual-channel output function generator (33522B, Agilent). A focused ultrasound transducer (V314, Panametrics-NDT) with fundamental frequency 0.89 MHz was used as detector. The detected signals were first amplified by a 40 dB pre-amplifier (5676, Parametrics-NDT) and then sent to a data-acquisition card (NI PXIe-5122) for signal processing. Fresh sterile heparinized sheep blood (CL2581-500H, Cederlane) was prepared and stored in the lab refrigerator at 4 °C. About 60 mL of the fresh blood was transferred into a 100 mL commercial blood bag (JB1302, Baxter) for each experiment. Eleven samples were prepared for experiments. The blood bag had two outlets connected to the circulation pump unit (5201, Heidolph)) with plastic tubing. One was connected to the sucking side and the other to the pushing side. The blood flow could continuously circulate in the system for over 5 h without coagulation. Sodium dithionite ($Na_2O_4S_2$, Sigma-Aldrich) was added into the blood circulation for deoxygenation [17]. The blood sample was injected into a B-cassette (BP7562, Opti Medical) and tested by a Blood Gas Analyzer (CCA-TS, Opti Medical). The S_tO_2 concentration of the sheep blood was measured before each scan. The oxygen saturation (S_tO_2) values were 95 %, 89 %, 87 %, 84 %, 80 %, and 73 %. The results of the differential PA signal amplitude dependence on power ratio $P_r = \frac{E_A}{E_B}$ (E_A and E_B are the power of laser A and B,

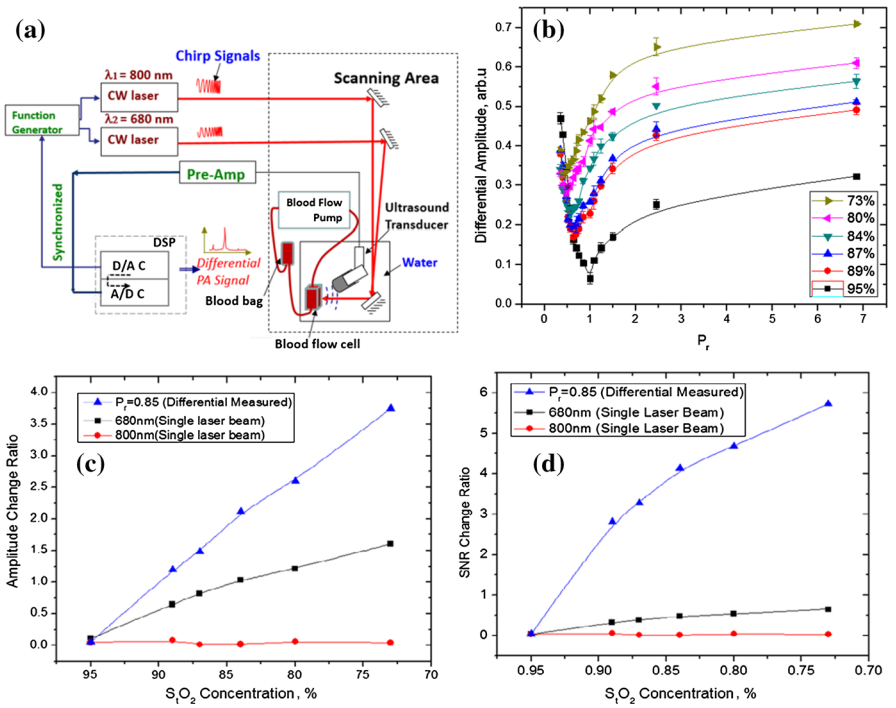

Fig. 5 (a) Experimental setup for wavelength-modulated differential FDPA radar system, (b) Differential amplitude of PAR signal with increasing P_r, (c) Differential and single-laser (680 nm or 800 nm) PA amplitude change ratio versus S_tO_2 concentration at power ratio $P_r = 0.85$, (d) PA relative SNR versus S_tO_2 concentration for differential and single-laser (680nm and 800nm) signals ($P_r = 0.85$)

respectively) are shown in Fig. 5b. It is seen that the differential amplitude changes with power ratio P_r and oxygen saturation. From the P_r scan result, it was found that the higher sensitivity was obtained for signal strength and relative SNR at $P_r = 0.85$. The relative signal sensitivity depends on the change ratio (CR) which is defined as

$$CR = \frac{Value_i - Value_0}{Value_0}, \tag{16}$$

where $Value_0$ is the initial measured PA signal (95 % S_tO_2 concentration), and $Value_i$ is the measured PA signal at a certain S_tO_2 concentration. The signal strength sensitivity comparison of the differential measurement with single-laser measurement is shown in Fig. 5c. The amplitude change ratio of single 800 nm laser excited PA signals exhibited only minimal change with decreasing concentration of S_tO_2, the 680nm laser excited PA signals exhibited higher change than 800nm, but lower than the differential results. The relative SNR comparison between differential PA and single-laser PA is shown in Fig. 5d. The differential PA results also showed higher SNR change ratio than single-laser excited PA.

4 Conclusions

A heating method was developed for enhancing PA radar imaging contrast. The experimental results showed that PA imaging contrast improved by 18.5 % from 32 °C to 38 °C. A differential chirp-signal modulation photoacoustic radar spectroscopy using for early cancer diagnosis was also developed. The two out-of-phase chirp-signals modulating two different wavelength laser beams (680 nm and 800 nm) suppressed the background noise significantly and increased signal sensitivity to hemoglobin oxygenation levels (S_tO_2) of sheep blood.

Acknowledgments A. M. gratefully acknowledges the support of NSERC through a Discovery Grant, and the support of the Samsung Advanced Institute of Technology (SAIT) through a Global Research Outreach (GRO) Research Project Grant.

References

1. D.A. Berry, K.A. Cronin, S.K. Plevritis, D.G. Fryback, L. Clarke, M. Zelen, J.S. Mandelblatt, A.Y. Yakovlev, J.D.F. Habbema, E.J. Feuer, Effect of screening and adjuvant therapy on mortality from breast cancer. N. Engl. J. Med. **353**, 1784–1792 (2005)
2. V.G. Andreev, A.A. Oraevsky, A.A. Karabutov, Wide-band acoustic pulse detection in opto-acoustic tomography system. Ultrason. Symp. 2000 IEEE **2**, 1205–1208 (2000)
3. W.F. Cheong, S.A. Prahl, A.J. Welch, A review of the optical properties of biological tissues. IEEE J. Quantum Electron. **26**, 2166–2185 (1990)
4. N. Won, S. Jeong, K. Kim, J. Kwag, J. Park, S.G. Kim, S. Kim, Imaging depths of near-infrared quantum dots in first and second optical windows. Mol. Imaging **11**, 338–352 (2012)
5. G. Kelly, Body temperature variability (Part 1): a review of the history of body temperature and its variability due to site selection, biological rhythms, fitness, and aging. Altern. Med. Rev. **11**, 278–293 (2006)
6. L.F. Fajardo, Pathological effects of hyperthermia in normal tissues. Cancer Res. **44**, 4826s–4835s (1984)
7. J. van der Zee, Heating the patient: a promising approach? Ann. Oncol. **13**, 1173–1184 (2002)
8. S.A. Sapareto, W.C. Dewey, Thermal dose determination in cancer therapy. Int. J. Radiat. Oncol. Biol. Phys. **10**, 787–800 (1984)
9. W. Wang, A. Mandelis, Thermally enhanced signal strength and SNR improvement of photoacoustic radar module. Biomed. Opt. Express **5**, 2785–2790 (2014)
10. I.V. Larina, K.V. Larin, R.O. Esenaliev, Real-time optoacoustic monitoring of temperature in tissues. J. Phys. **38**, 2633–2639 (2005)
11. R. Splinter, *An Introduction to Biomedical Optics* (Taylor & Francis, London, 2007)
12. M. Hockel, P. Vaupel, Tumor hypoxia: definitions and current clinical, biologic, and molecular aspects. J. Natl Cancer Inst. **93**, 266–276 (2001)
13. A.J. Comerota, R.C. Throm, P. Kelly, M. Jaff, Tissue (muscle) oxygen saturation (S_tO_2): a new measure of symptomatic lower-extremity arterial disease. J. Vasc. Surg. **38**, 724–729 (2003)
14. R. Esenaliev, I. Larina, K. Larin, D. Deyo, M. Motamedi, D. Prough, Optoacoustic technique for noninvasive monitoring of blood oxygenation: a feasibility study. Appl. Opt. **41**, 4722–4731 (2002)
15. V.E. Gusev, A.A. Karabutov, *Laser Optoacoustics* (American Institute of Physics, New York, 1993)
16. M.S. Patterson, F.S. Foster, The improvement and quantitative assessment of B-mode images produced by an annular array/cone hybrid. Ultrason. Imaging **5**, 195–213 (1983)
17. B. Yin, R.V. Kuranov, A.B. McElroy, S. Kazmi, A.K. Dunn, T.Q. Duong, T.E. Milner, Dual-wavelength photothermal optical coherence tomography for imaging microvasculature blood oxygen saturation. J. Biomed. Opt. **18**, 056005 (2013)